Advances in Applied Mathematics and Mechanics
Adv. Appl. Math. Mech., Vol. **9**, No. 2, pp. 233-249

DOI: 10.4208/aamm.2015.m1376
April 2017

The Motion of a Neutrally Buoyant Ellipsoid Inside Square Tube Flows

Xin Yang, Haibo Huang* and Xiyun Lu

Department of Modern Mechanics, University of Science and Technology of China, Hefei, Anhui 230026, China

Received 21 December 2015; Accepted (in revised version) 26 February 2016

Abstract. The motion and rotation of an ellipsoidal particle inside square tubes and rectangular tubes with the confinement ratio $R/a \in (1.0,4.0)$ are studied by the lattice Boltzmann method (LBM), where R and a are the radius of the tube and the semi-major axis length of the ellipsoid, respectively. The Reynolds numbers (Re) up to 50 are considered. For the prolate ellipsoid inside square and rectangular tubes, three typical stable motion modes which depend on R/a are identified, namely, the kayaking mode, the tumbling mode, and the log-rolling mode are identified for the prolate spheroid. The diagonal plane strongly attracts the particle in square tubes with $1.2 \leq R/a < 3.0$. To explore the mechanism, some constrained cases are simulated. It is found that the tumbling mode in the diagonal plane is stable because the fluid force acting on the particle tends to diminish the small displacement and will bring it back to the plane. Inside rectangular tubes the particle will migrate to a middle plane between short walls instead of the diagonal plane. Through the comparisons between the initial unstable equilibrium motion state and terminal stable mode, it is seems that the particle tend to adopt the mode with smaller kinetic energy.

AMS subject classifications: 65M99, 76D99

Key words: LBM, Poiseuille flow, square tubes, ellipsoidal particles.

1 Introduction

The motion of the particles in tubes are ubiquitous in nature and many applications in industries, such as chemical, biological, and mechanical engineering. Many studies on the motion of particles in simple flows have been carried out, for example, the particle's rotational behaviors in Couette flow [1–6], sedimentation of particles inside tubes [7]. Here we focus on the particle's behaviors in tube flows.

*Corresponding author.
Email: Yangxin@mail.ustc.edu.cn (X. Yang), huanghb@ustc.edu.cn (H. B. Huang), xlu@ustc.edu.cn (X. Y. Lu)

In 1961, Segre and Silberberg studied the migration of neutrally buoyant spherical particles in Poiseuille flows experimentally and found that the particles migrate towards an equilibrium position and equilibrate at a distance of 0.6 time the radius of the tube from the tube's center [8]. In one hand, the particle experiences the "Magnus effect" due to the rotation of the particle. The rotation of the particle is induced by the shear stress in the Poiseuille flow. When the particle migrates radially to the wall, the fluid between the wall and the particle is squeezed and inversely, the particle will experience high pressure to prevent it to reach the wall. Hence, the particle will seek an equilibrium position between the axis and the wall where the total radial force is zero. Karnis et al. [9] studied the migration of non-spherical particles in tubes in 1966. They observed that for a rod-like particle, the major axis of the particle rotates on the plane passing though the center of the particle and the tube axis (tumbling state), while for a disk-like particle, it rotates with its minor axis on the same plane (log-rolling state).

Feng and Joseph simulated the motion of a single ellipse in two-dimensional (2D) creeping flows using a Finite Element (FE) method [10]. According to their study, a neutrally buoyant particle exhibits the Segre-Silberberg effect in a Poiseuille flow. The driving forces of the migration have been identified as a wall repulsion due to lubrication, an inertial lift related to shear slip, a lift due to particle rotation and the velocity profile curvature. By examining the pressure and shear stress distributions on the particle, they found that the stagnation pressure on the particle surface are particularly important in determining the direction of migration.

Yang et al. [11] simulated a single neutrally buoyant spherical particle in tube flows and they used a method of constrained simulation to obtain correlation formulas for the lift force, slip velocity, and equilibrium position.

Sugihara-Seki numerically studied the motions of an inertialess elliptical particle in tube Poiseuille flow using a Finite Element (FE) method [12]. A prolate spheroid is found to either tumble or oscillate in rotation, depending on the particle-tube size ratio, the axis ratio of the particle, and the initial conditions. A large oblate spheroid may approach asymptotically a steady, stable slightly inclined configuration, at which it is located close to the tube centreline.

However, in the paper they consider only the motion where two of the three principal axes of the ellipsoid lie in a plane containing the tube axis and the fluid motion is assumed to be symmetric with respect to this plane. On the other hand, the inertia of the particle is very important in this flow problem but it is not considered. Hence it is only a starting point for the analysis of the general motion of an ellipsoid in tube flows.

Yu et al. studied the the migration in a Poiseuille flow using a finite-difference-based DLM method [13]. They found that suppression of the sphere rotation produces significant large additional lift forces pointing towards the tube axis on the spheres in the neutrally buoyant cases.

Pan et al. [14] simulated the motion of a neutrally buoyant ellipsoid in a Poiseuille flow and investigated its rotational and orientational behavior inside circular tubes. However, the study only considered circular tubes with fixed $R/a \approx 3$.

For cases with $Re=5.4$, $R/a\approx 2.5$, the prolate ellipsoid's long axis rotates on the plane passing through the cylinder axis and its mass center. This behavior is similar to the experimental results of the rod-like particle moving and rotating in the Poiseuille flow reported in [9]. This is called the tumbling mode.

For cases with $Re=26.23$ and 50.9, the prolate ellipsoid has two different rotational behaviors after reaching its equilibrium distance to the central axis of the tube. The prolate ellipsoid is rotating with respect to its long axis, which is perpendicular to the plane passing through the central axis of the tube and its mass center. That is the log-rolling state. This was not reported in [9]. The tumbling mode may also appear for special initial orientation and positions.

For the oblate ellipsoid and $R/a\approx 3.3$, the oblate ellipsoid rotates with its short axis perpendicular to the plane passing through the central axis of the tube and the mass center of the disk. That is a log-rolling mode for $Re<81$. The behavior is similar to the experimental results for the disk-like particle moving and rotating in the Poiseuille flow reported in [9].

In this paper, the migration and rotation in Poiseuille flows inside square tubes are investigated in detail. Besides, rectangular tubes are also considered. Hence, the main emphasis in this work is to study the effect of wall boundaries on the ellipsoid behaviors in tubes flows.

We try to understand the behavior of the particle according to the kinematic energy of the particle, which is in a similar way to Jeffery. Jeffery theoretically investigated the rotational modes of an ellipsoid under Stokes flow conditions. Because the final rotational state of an ellipsoid may depend on initial conditions, Jeffery hypothesized that: "The particle will tend to adopt that motion which, of all the motions possible under the approximated equations, corresponds to the least dissipation of energy".

In Section 2, the MRT LBM and basic equations for the motion of the solid particle are introduced briefly. The identified modes are discussed in Section 4. Finally, some conclusion remarks are stated in Secion 5.

2 Numerical method

2.1 Multiple-Relaxation-Time (MRT) Lattice Boltzmann method

The MRT-LBM [15] is used to solve the fluid flow governed by the incompressible Navier-Stokes equations. The LBE [16] can be written as

$$|f(\vec{x}+\vec{e}_i\delta t,t+\delta t)\rangle-|f(\vec{x},t)\rangle=-\mathbf{M}^{-1}\hat{\mathbf{S}}\left[|m(\vec{x},t)\rangle-|m^{eq}(\vec{x},t)\rangle\right], \tag{2.1}$$

where Dirac notation of ket $|\cdot\rangle$ vectors symbolize the column vectors. $|f(\vec{x},t)\rangle$ represents the particle distribution function which has 19 component f_i with $i=0,1,\cdots,18$, because of the D3Q19 model used in our 3D simulations. The collision matrix $\hat{\mathbf{S}}=\mathbf{M}\cdot\mathbf{S}\cdot\mathbf{M}^{-1}$ is diagonal with

$$\hat{\mathbf{S}}\equiv(0,s_1,s_2,0,s_4,0,s_4,0,s_4,s_9,s_{10},s_9,s_{10},s_{13},s_{13},s_{13},s_{16},s_{16},s_{16}), \tag{2.2}$$

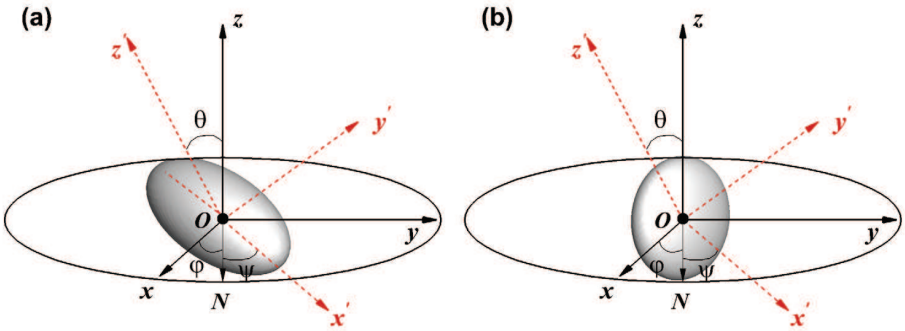

Figure 1: Schematic diagram of the combination of coordinate transformation from (x,y,z) to (x',y',z') with three Euler angles (ϕ,θ,ψ). Line "ON" represents the pitch line of (x,y) and (x',y') coordinate planes. Two coordinate systems are overlapping initially. First the particle rotates around the z' axis with a recession angle ϕ and then the particle rotates around the new x' axis (i.e., line "ON") with a nutation angle θ. Finally the particle rotates around the new z' axis with a angle of rotation ψ.

where the parameters of $\hat{\mathbf{S}}$ are chosen as [16]: $s_1=1.19$, $s_2=s_{10}=1.4$, $s_4=1.2$, $s_9=1/\tau$, $s_{13}=s_9$, $s_{16}=1.98$. $|m^{eq}\rangle$ is the equilibrium value of the moment $|m\rangle$, where the moment $|m\rangle=\mathbf{M}\cdot|f\rangle$, i.e., $|f\rangle=\mathbf{M}^{-1}\cdot|m\rangle$. $\mathbf{M}$ is a 19×19 linear transformation matrix which is used to map the column vectors $|f\rangle$ in discrete velocity space to the column vectors $|m\rangle$ in moment space. The matrix $\mathbf{M}$ and $|m^{eq}\rangle$ are same with those used by D'Humiere et al. [16] and Huang et al. [4]. In Eq. (2.1), $\vec{e}_i$ are the discrete velocities. For the D3Q19 velocity model,

$$\vec{e}_i=c\begin{bmatrix}0&1&-1&0&0&0&0&1&1&-1\\0&0&0&1&-1&0&0&1&-1&1\\0&0&0&0&0&1&-1&0&0&0\\-1&1&-1&1&-1&0&0&0&0&\\-1&0&0&0&0&1&1&-1&-1&\\0&1&1&-1&-1&1&-1&1&-1&\end{bmatrix}, \tag{2.3}$$

where c is the lattice speed defined as $c=\Delta x/\Delta t$. In our study $\Delta x=1lu$ and $\Delta t=1ts$, where lu, ts, mu represent the lattice unit, time step, and mass unit, respectively. The macro-variables of fluid flow can be obtained from

$$\rho=\sum_i f_i,\quad \rho u_\alpha=\sum_i f_i e_{i\alpha},\quad p=c_s^2\rho, \tag{2.4}$$

where subscript α denotes three coordinates. The parameter τ is related to the kinematic viscosity of the fluid: $\nu=c_s^2(\tau-0.5)\Delta t$, where $c_s=c/\sqrt{3}$ is the sound speed.

The numerical method used in our study is based on the MRT-LBM [16] and the dynamic multi-block strategy [17]. The numerical methods are validated in [17].

2.2 Solid particle dynamics and fluid-solid boundary interaction

In our simulation, the ellipsoidal particle is described by

$$\frac{x'^2}{a^2}+\frac{y'^2}{b^2}+\frac{z'^2}{c^2}=1, \tag{2.5}$$

where a, b, and c are the lengths of three semi-principal axes of the particle in x', y', and z' axis of body-fixed coordinate system, respectively (see Fig. 1). The body-fixed coordinate system can be obtained by a combination of coordinate transformation around the $z'-x'-z'$ axis with Euler angles (ϕ,θ,ψ) from space-fixed coordinate system (x,y,z) which initially overlaps the body-fixed coordinate system. The combination of coordinate transformation is illustrated in Fig. 1. The evolution axis always overlaps the x' direction. The migration and rotation of the particle are determined by Newton's equation and Euler's equation

$$m\frac{d\mathbf{U}(t)}{dt}=\mathbf{F}(t), \tag{2.6a}$$

$$\mathbf{I}\cdot\frac{d\mathbf{\Omega}(t)}{dt}+\mathbf{\Omega}(t)\times[\mathbf{I}\cdot\mathbf{\Omega}(t)]=\mathbf{T}(t), \tag{2.6b}$$

where $\mathbf{I}$ is the inertial tensor, and $\mathbf{\Omega}(t)$ and $\mathbf{T}$(t) represent the angular velocity and the torque exerted on the particle in the body-fixed coordinate system, respectively. In the frame, $\mathbf{I}$ is diagonal and the principal moments of inertial can be written as

$$I_{x'x'}=m\frac{b^2+c^2}{5},\quad I_{y'y'}=m\frac{c^2+a^2}{5},\quad I_{z'z'}=m\frac{a^2+b^2}{5}, \tag{2.7}$$

where $m=4\rho_p\pi abc/3$ is the mass of the particle. ρ_p is the density of the particle. It is not appropriate to solve Eq. (2.6b) directly due to an inherent singularity [21]. Thus four quaternion parameters are used as generalized coordinates to solve the corresponding system of equations [3]. A coordinate transformation matrix with four quaternion parameters [3] is applied to transform corresponding item from the space-fixed coordinate system to the body-fixed coordinate system. With four quaternion parameters, Eq. (2.6b) can be solved using a fourth-order accurate Runge-Kutta integration procedure [4].

In the simulations, the fluid-solid boundary interaction is based on the schemes of Aidun et al. [2] and Lallmand and Luo [15]. The accurate moving-boundary treatment proposed by Lallmand and Luo [15] is applied to solve the problem caused by the moving curved-wall boundary condition of the ellipsoid.

The general schemes for calculation of interactive force between fluid and particle in the LBM include stress integration, momentum exchange and volume fraction models. That has been summarized and analysed in [18]. The stress integration scheme may be good but it is not so efficient [18]. Here the momentum exchange scheme is used to calculate the force exerted on the solid boundary, which is accurate and efficient. The

forces due to the fluid nodes covering the solid nodes and the solid nodes covered by the fluid nodes [2] are also considered in the study.

To prevent the overlap of the particle and the wall, usually the repulsive force between the wall and particle should be applied [17]. Here the lubrication force model is identical to that we used in [17] and the validation of the force model has been tested extensively in [17].

Our LBM code has been validated in [17] by the migrations of a neutrally buoyant sphere in tube Poiseuille flows [9] and a prolate ellipsoid sedimentation in a circular tube [19]. To further validate our LBM code, the migration of a neutrally buoyant sphere in a tube Poiseuille flow is also performed [20].

3 Flow problem

The motion of a neutrally buoyant ellipsoid inside square tube flow is illustrated in Fig. 2, where $D=2R$ denotes the width of the square tube. In the problem, two kinds of ellipsoids, the prolate and the oblate particles, are considered. The particle size $a=2b=2c$ for the prolate particle and $2a=b=c$ for the oblate ellipsoid are considered. (x',y',z') are body-fixed coordinates. The x' axis is fixed on the particle where it overlaps the major axis of the prolate particle and the minor axis of the oblate. The Reynolds number (Re) is defined as $Re=aU_m/\nu$, where U_m is the central velocity of the flow without the particle. The confinement ratio is R/a.

For all cases in our study, the length of the square tube is $L=8D$ so that the effects of the inlet/outlet boundary conditions are minimized. In most simulations, the semi-major axis of the ellipsoidal particle is represented by $20lu$, i.e., $a=20lu$ and $\tau_f=0.6$. For example, in the case of $R/a=1.2$, the total mesh is about $50lu\times 50lu\times 400lu$. The grid independence study and time step independence study have been performed and it is shown that the mesh size and the time step are sufficient to get accurate results.

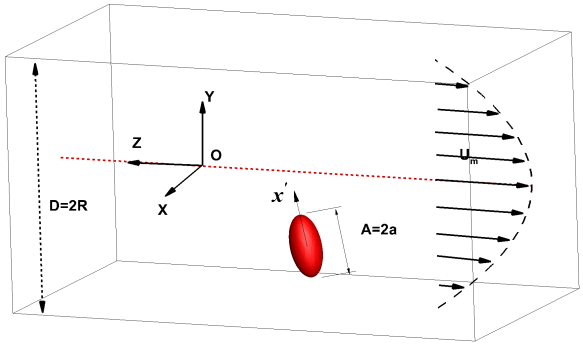

Figure 2: Schematic diagram for the motion of an ellipsoid inside square tube flow.

4 Discussion

Both the prolate and the oblate ellipsoids inside square tubes are considered in the study. Simulations of cases with different Re and confinement ratio R/a are performed, three modes are found, namely, the tumbling mode, the log-rolling mode, and the kayaking mode. In the following, the modes are discussed in detail.

4.1 Motion and rotation of a prolate particle

4.1.1 The effect of the confinement ratio R/a

The confinement ratio R/a plays a significant role in the rotation and migration of the particle in the square tube flow. Our results show that there exist three modes, namely, kayaking, log-rolling, and tumbling modes in the range $1.0 \leq R/a \leq 4.0$. Fig. 3 shows the schematic diagram of these modes. (I) to (IV) are the kayaking mode, the log-rolling mode with x' axis perpendicular to the diagonal plane, the tumbling mode on the diagonal plane, and the tumbling mode on a middle plane parallel to the wall.

(I) Regime I ($1.0 \leq R/a < 1.2$)

Firstly, the particle's behavior inside very narrow tubes is investigated. Due to the Segre-Silberberg effect, the prolate ellipsoid will migrate to an equilibrium position between the tube axis and the wall. It will eventually reach the kayaking mode. In the mode, the particle rotates around the x' axis with precession and nutation (see Fig. 3(I)) between the tube axis and the wall. It looks like a paddle kayaking around its equilibrium position with small amplitude.

Fig. 4 shows the evolutions for normalized x and y of the particle center and the orientation of the x' axis. The length, time, and velocities are normalized by R, U_m/a and U_m, respectively. It is seen that finally the mass center of the particle is inside the $y=0$ plane with small oscillations. Due to the precession and nutation, $\cos\alpha$ and $\cos\gamma$ would

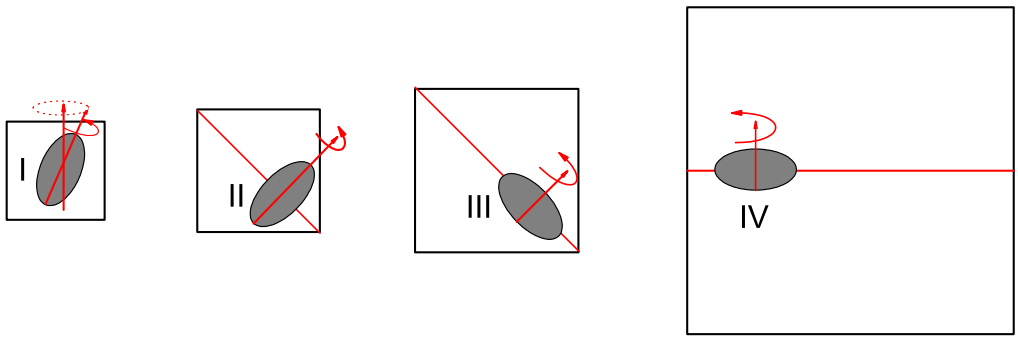

Figure 3: The schematic diagram of the modes in the four regimes in the flow direction. I to IV represent the kayaking mode, the log-rolling mode with x' axis perpendicular to the diagonal plane, the tumbling mode on the diagonal plane, and the tumbling mode on the plane parallel to the wall, respectively.

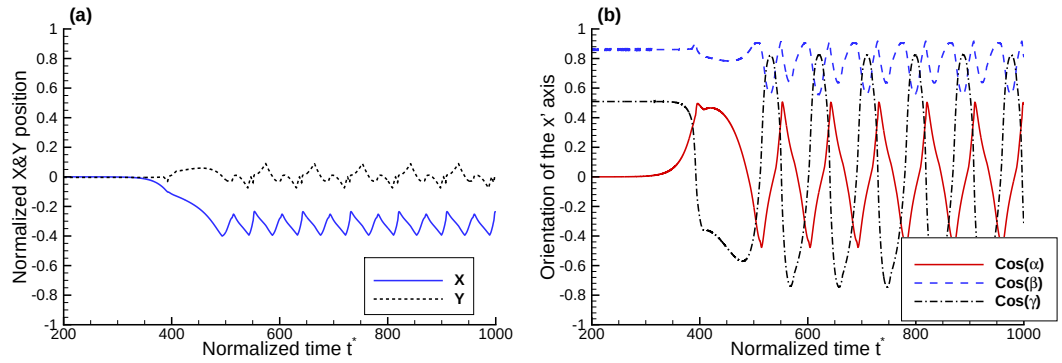

Figure 4: Kayaking mode ($R/a=1.0,\ Re=10$). (a) The normalized x and y positions of the center of the particle as functions of time. (b) The orientation of the x' axis as a function of time.

change periodically and the oscillation of $\cos\beta$ may be caused by the y-oscillation of the particle center.

For most initial conditions, the prolate ellipsoid usually migrate and rotate in the kayaking mode. However, when the x' axis of the prolate ellipsoid is initially close to the diagonal plane, the particle may migrate and rotate in the tumbling mode on the diagonal plane finally.

(II) Regime II ($1.2\leq R/a<1.8$)

A tube that is slightly wider ($1.2\leq R/a<1.8$) than that in Regime I. In this regime, the log-rolling mode can be observed (see Fig. 3(II)). In the log-rolling mode, the particle rotates around its evolution axis (x' axis) which is almost perpendicular to the diagonal plane and move along the flow at its equilibrium position. Fig. 5 shows the result of a typical case in this regime. In the case, initially the particle rotates in the tumbling mode

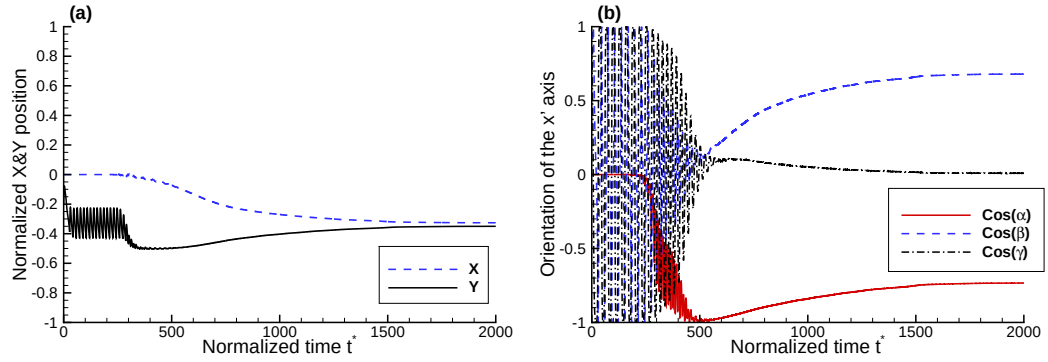

Figure 5: Log-rolling mode with the x' axis perpendicular to the diagonal plane ($R/a=1.5,\ Re=50$). (a) The normalized x and y positions of the center of the particle as functions of time. (b) The orientation of the x' axis as a function of time.

around its minor axis ($t^* < 500$) and the x' axis is parallel to the wall, later the x' axis becomes perpendicular to the diagonal plane ($\cos\gamma = 0$, $\cos\alpha = -0.707$, $\cos\beta = 0.707$). Hence, in most cases, the particle will be attracted by the diagonal plane.

However, when the x' axis of the prolate ellipsoid is initially close to the diagonal plane, the tumbling mode on the diagonal plane appears again, which is similar to that in Regime I.

(III) Regime III ($1.8 \leq R/a \leq 3.0$)

When R/a is moderate ($1.8 \leq R/a \leq 3.0$), the prolate ellipsoid would generally reach the tumbling mode with x' axis inside the diagonal plane of the square tube (see Fig. 3(III)).

The log-rolling mode may also appear under special initial conditions, for example, the x' axis of the prolate ellipsoid is set to be parallel to the wall and perpendicular to the tube axis initially. However, the log-rolling mode is unstable and with a small disturbance the initial log-rolling mode will transfer to the tumbling mode with the x' axis in the diagonal plane.

Fig. 6 shows a typical result. Initially, the x' axis of the prolate ellipsoid is inside the (y,z) plane with $x = 0$. At beginning ($t^* < 2000$), the prolate ellipsoid is tumbling on

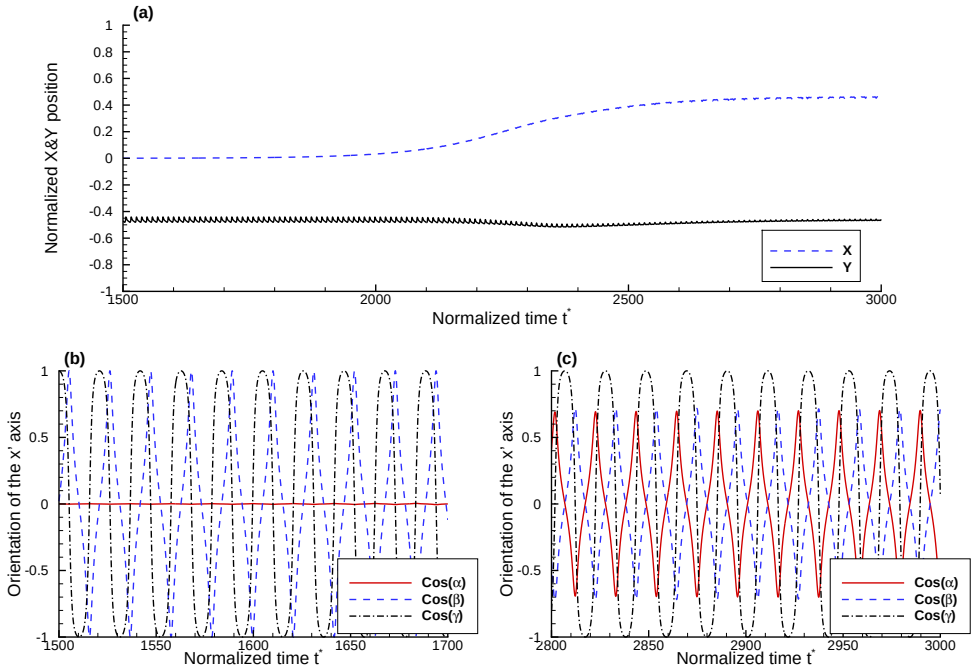

Figure 6: Tumbling mode in the diagonal plane ($R/a = 2.0$, $Re = 10$). (a) The normalized x and y positions of the center of the particle as functions of time. (b) and (c) show the orientation of the x' axis as a function of time. The prolate particle rotates on the plane parallel to the wall when $1500 < t^* < 1700$ (see (b)) while on the diagonal plane when $2800 < t^* < 3000$ (see (c)).

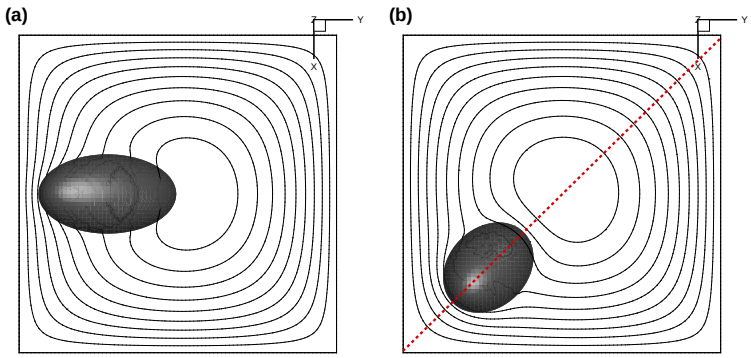

Figure 7: The contour lines of the flow velocity for the tumbling mode on (a) the plane parallel to the wall initially, and (b) the diagonal plane of the tube finally ($R/a=2.0$, $Re=10$). The origin of the coordinates is at the center of the square.

the plane. However, it is unstable and eventually the prolate ellipsoid migrates to the diagonal plane after $t^*>2000$.

The contour lines of the flow velocity are also shown in Fig. 7. As mentioned in Fig. 6, the x' axis of the prolate ellipsoid is on the $x=0$ plane initially. The flow is symmetric about the $x=0$ plane and the tumbling state in the the $x=0$ plane is an equilibrium state.

However, the tumbling in the $x=0$ plane is unstable. A small displacement from the plane will break the symmetry of the streamlines. Because the the shear rate is no longer symmetric about the x' axis, the particle may experience a force to push it away from its initial symmetric plane until it reaches the diagonal plane, which is another equilibrium plane. From Fig. 7(b), it is seen that the shear rate is also symmetric about the x' axis when the particle is inside the diagonal plane. The diagonal plane is the stable equilibrium position and even with a disturbance, the particle will be attracted to the diagonal plane again.

To explore the mechanism why the tumbling mode is stable in the diagonal plane instead of the middle plane parallel to the walls (see Fig. 6), some constrained cases are simulated. In the constrained cases, the particle rotates freely but only allowed to move along a line parallel to the axis of the tube. The lateral migration is suppressed.

First we studied constrained cases with a small displacement Δ from the $x=0$ plane. Suppose in the initial equilibrium tumbling state, the position of the center of the particle is $(0,y_0)$ (see Fig. 7(a)). In these constrained cases, the center of the particle is fixed in (Δ,y_0), i.e., the particle is only allowed to move along the line parallel to the z axis. It is found that the constrained particle almost adopts a tumbling mode. Several cases with different Δ are simulated. The result is shown in Fig. 8. It is seen that the total force acting on the particle ($F0$) has same sign as Δ. Hence, the force due to a small disturbance will push the particle away from the $x=0$ plane rather than bring it back to the $x=0$ plane. In other words, the force will amplify the small disturbance.

Second we studied constrained cases with a small displacement Δ from the diagonal

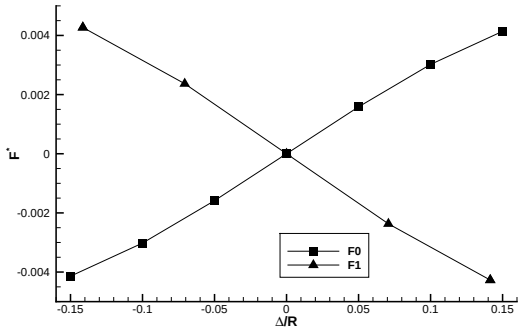

Figure 8: The force acting on the prolate particle in constrained cases $F0$ and $F1$ as functions of small displacements Δ from $x=0$ plane and from the diagonal plane, respectively. In the cases $R/a=2.0$, $Re=10$.

plane. Suppose in the stable tumbling state, the center of the particle is at (x_0,y_0) (see Fig. 7(b)). In the constrained cases, the center of the particle is fixed in $(x_0-\Delta,y_0+\Delta)$, i.e., the particle is only allowed to move along the z axis. The constrained particle will still adopts a tumbling mode. The result is shown in Fig. 8. It is seen that the sign of the force acting on the particle ($F1$) is opposite to Δ, i.e., the force tends to diminish the small displacement and will bring it back to the diagonal plane. Hence, the tumbling mode is stable in the diagonal plane.

(IV) Regime IV ($R/a>3.0$)

For wider tubes, when initially the x' axis is parallel to the wall and perpendicular to the tube's axis, the log-rolling mode may appear. However, the log-rolling mode may be unstable and even with a small disturbance, it may transfer to the tumbling mode, which is similar to the phenomenon in Regime III. Fig. 9 shows this transitional procedure from the initial log-rolling mode to the tumbling mode.

For the other initial positions and orientations, eventually the particle will reach the tumbling mode. For the tumbling mode in this regime, the x' axis is inside the plane passing through the initial center of the particle and the tube axis. That is slightly different from the tumbling in Regime III, in which the x' axis is always in the diagonal plane. Due to a big R/a, the wall effect is very weak so that the particle can rotate on the plane parallel to the wall stably. Hence, the diagonal plane effect is not strong as that in Regime III.

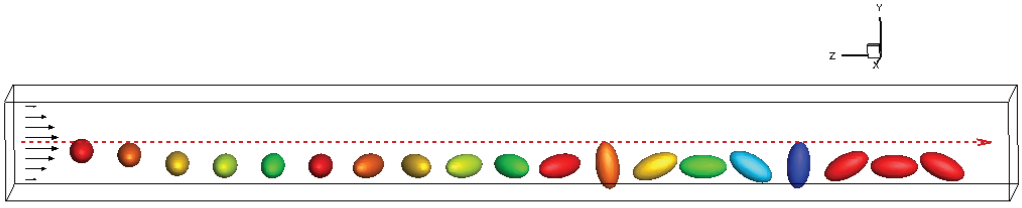

Figure 9: The mode transformation from the log-rolling mode to the tumbling mode for the prolate ellipsoid.

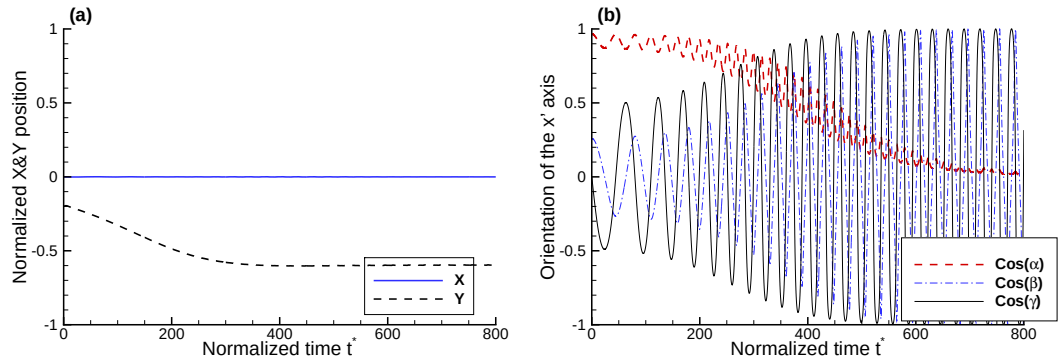

Figure 10: Tumbling mode on the plane parallel to the wall ($R/a=4.0$, $Re=10$). (a) The normalized x and y positions of the center of the particle as a function of time. (b) The orientation of the x' axis as a function of time.

As a small conclusion, the effect of the confinement ratio R/a plays a significant role for the flow pattern of the prolate ellipsoid. It also determines the strength of the diagonal effect that ellipsoid is attracted to the diagonal plane of the square tube. From the above discuss, it is seen that the effect is strong just in the moderate wide square tube $1.2<R/a<3.0$.

For the other regimes, the diagonal effect is not so strong, i.e., only when the particle is close to the diagonal plane, it will be attracted.

For the much wider square tubes beyond the above cases, the wall effect is very weak. The prolate particle may rotate stably on the plane parallel to the wall (see Fig. 10). It is not attracted by the diagonal plane and the motion mode of the particle inside the square tube is similar to that in a circular tube [14].

For the narrow square tubes, the wall effect becomes stronger so that the interaction between the particle and the fluid is complex. A complicated mode as Kayaking mode will appear.

In our study, it is found that the equilibrium position, the migration velocity, and the angular velocity depend on Re. With Re increasing, the equilibrium position is closer to the wall of the tube, and the normalized migration velocity of the particle along the tube axis becomes smaller and the normalized angular velocity increases.

4.1.2 Tube geometry effect

We also further investigated the tube geometry effect. A rectangular tube with dimensions of $2R$ and $4R$ in the x and y-direction, respectively, is considered. We would like to see whether the particle will be attracted to the diagonal plane.

The tumbling mode and the log-rolling mode can be observed. The rotation mode in the rectangular tubes depends on the initial orientation and position of the ellipsoid. Here two typical cases (Case I and Case II) are simulated. In both cases, The x' axis is inside the middle (x,z) plane of the tube with initial position $(x_0,y_0)=(0,-0.4)$. The

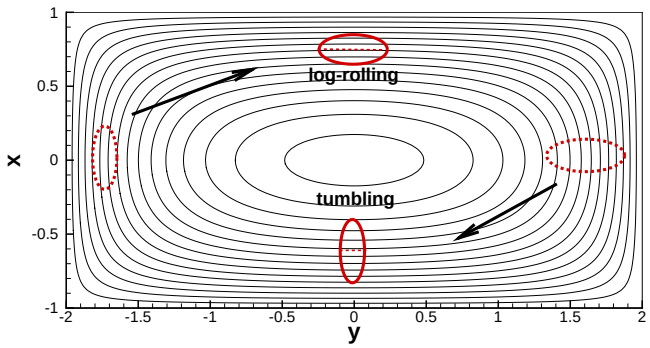

Figure 11: Top-view of the contours of the velocity magnitude without particle. The dashed ellipsoid represents the initial position of the prolate particle and the solid ellipsoids are the final tumbling mode and the log-rolling mode.

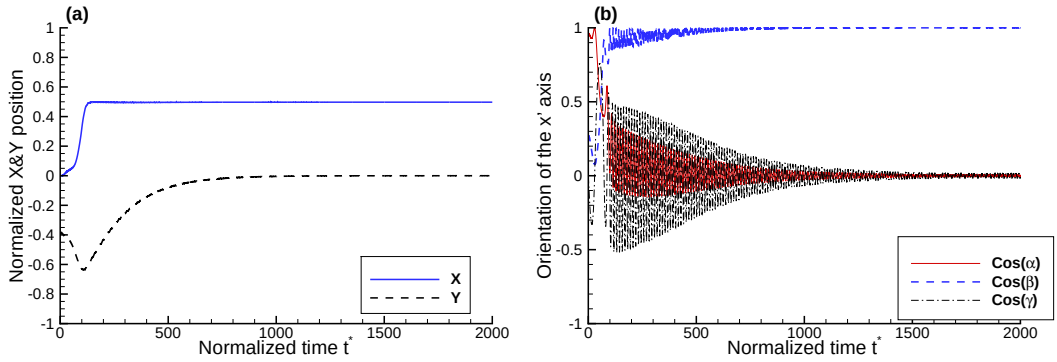

Figure 12: The log-rolling mode for a prolate ellipsoid inside the rectangular tube (Case I, $R/a=2.0$, $Re=10$, $\gamma=0^\circ$). (a) The normalized x and y positions of the center of the particle as a function of time. (b) The orientation of the x' axis as a function of time.

dashed ellipsoid shown in Fig. 11 represents the initial position of the ellipsoid. In case I, $\alpha=0^\circ,\gamma=90^\circ$, i.e., the x' axis is parallel to the x axis. In Case II, $\alpha=90^\circ,\gamma=75^\circ$. Consider the Segre-Silberberg effect, it is conjectured that the particle may adopt the log-rolling or tumbling mode with an equilibrium position. However, the particle will leave the initial plane. Due to asymmetry of the shear rate near the diagonal plane, the diagonal plane is impossible to be the equilibrium plane. The particles will gradually shift to the middle (x,z)-plane in both cases.

The evolutions of the position and orientation of the particle for Case I are shown in Fig. 12. Finally, the major axis (x' axis) is consistent with the y axis.

The evolution of the particle position and orientation for Case II are shown in Fig. 13. Initially the prolate particle is still released from $(x,y)=(0,-0.4)$ and the x' axis of the particle is inside the (y,z)-plane but not perpendicular to the z-direction, e.g., $\gamma=75^\circ$. From Fig. 13, it is seen that a tumbling mode appears. Due to the Segre-Silberberg effect,

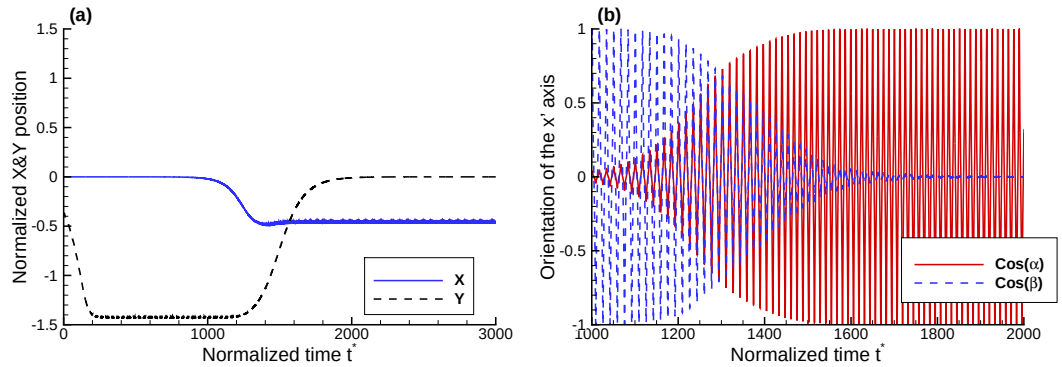

Figure 13: The tumbling mode for a prolate ellipsoid inside the rectangular tube (Case II, $R/a=2.0$, $Re=10$, $\gamma=75°$). (a) The normalized x and y positions of the center of the particle as functions of time. (b) The orientation of the x' axis as a function of time.

the ellipsoid migrates to its equilibrium position ($(x,y)=(0,-1.4)$) at $t\approx 200$. But the tumbling state inside the (y,z)-plane is unstable. The x' axis of the prolate ellipsoid gradually transfers to the (x,z)-plane without mode change. The terminal schematic diagram is show in Fig. 11.

4.2 Motion and rotation of an oblate particle

We also carried out simulations for an oblate ellipsoid inside the square tubes. It is found only the log-rolling mode is stable. In the mode, the oblate particle rotates around its x' axis (the minor axis).

A typical translation and rotation behavior inside a square tube is shown in Fig. 14. Initially the particle rotates around its major axis, which looks like the tumbling state. Gradually it changes to the log-rolling mode. Here because the tube is not so wide, the diagonal effect may be not so strong and its x' axis seems parallel to the x axis. This terminal mode is stable. On the other hand, for a narrow tube, the particle may be attracted to the diagonal plane and in the log-rolling mode, its minor axis (x' axis) is perpendicular to the diagonal plane.

The equilibrium position, the migration velocity, and the angular velocity depend on

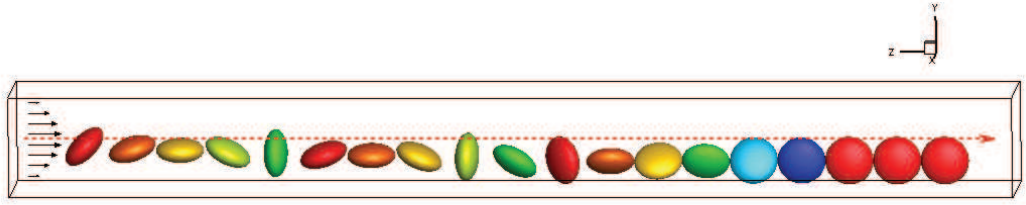

Figure 14: Motion of an oblate ellipsoid inside a square tube Poiseuille flow.

Re. With *Re* increasing, the equilibrium position is closer to the wall of the tube, and the corresponding non-dimensional migration velocity of the particle along the tube axis becomes small.

4.3 The kinetic energy of the particle

To explore the mechanism why the ellipsoid adopts a specific mode on the diagonal plane, the kinetic energies of an initial unstable equilibrium motion mode and the terminal stable state are calculated for comparison. The kinetic energy E is calculated as the summation of the translational energy and rotational energy.

Here we mainly studied the cases with initial tumbling state inside a middle plane parallel to the walls and tube size is $1.8 < R/a \leq 2.5$. As discussed in the above, the initial tumbling state is an unstable equilibrium motion mode and eventually the particle will be tumbling inside the diagonal plane, specifically, the kinetic energy E is

$$E = \frac{1}{2} m \mathbf{U}^2 + \frac{1}{2} I_{y'y'} \omega_{y'}^2. \tag{4.1}$$

During the evolution, the rotational mode of the prolate ellipsoid is almost tumbling and the plane containing x' axis gradually approaches to the diagonal plane (see Fig. 6).

Six such cases with different *Re* and R/a are simulated. Table 1 shows the results. The kinetic energy is normalized by $0.5mU_m^2$, where m is the mass of the particle and U_m is the maximal velocity in the fluid. It is seen that the kinetic energy of the particle decreases from the initial unstable equilibrium state to the stable mode.

Besides the above six cases, the other two cases (Cases A and B) are also investigated. In Case A, the prolate ellipsoid is inside the square tube with $R/a = 1.0$, $Re = 10$ and initially it is a log-rolling state in the center of the tube. Eventually it reaches the kayaking mode (see Fig. 4). The initial kinematic energy is $E_0 = 0.4775$ while the terminal kinematic energy is $E_1 = 0.3717$. It is seen that the kinematic energy decreases.

In Case B, a prolate ellipsoid is inside the square tube with $R/a = 1.2$, $Re = 10$, the initial unstable equilibrium state is tumbling mode inside a middle plane between two parallel walls. Finally it reaches the log-rolling mode with x' axis almost perpendicular to diagonal plane. The initial and terminal kinematic energies are $E_0 = 0.6368$ and $E_1 =$

Table 1: The kinetic energy of the prolate ellipsoid in an initial unstable equilibrium motion mode (E_0) and the terminal stable mode (E_1).

Re	R/a	E_0	E_1
10	2.0	0.5198	0.3540
20	2.0	0.6368	0.4019
30	2.0	0.7832	0.4706
10	2.5	0.4664	0.3524
20	2.5	0.4758	0.3753
30	2.5	0.4915	0.3842

0.2613, respectively. Hence, it also seems the particle tends to adopt a stable mode with smaller kinematic energy.

5 Conclusions

The motion and rotation of an ellipsoidal particle inside narrow square tubes and rectangular tubes have been studied numerically. Three modes are identified for prolate spheroid, namely, the kayaking mode, the tumbling mode, and the log-rolling mode. It is found that the geometric effect of the tube (R/a) plays a critical role for the motion mode. The log-rolling mode is the only stable mode for the oblate ellipsoid. The diagonal plane strongly attracts the particle in square tubes $1.2 < R/a < 3.0$.

It is found that the tumbling mode in the diagonal plane is stable because the shear stress acting on the particle will bring it back to the plane when there is a small disturbance. However, the tumbling state in a middle plane parallel to the walls is unstable, because the force will amplify the small disturbance.

In a the rectangular tube, there are no diagonal effect and the particle tends to be tumbling in the middle plane between two short walls or log-rolling with x' axis perpendicular to the plane.

Through the comparisons between the initial unstable equilibrium motion mode and terminal stable mode, it is seems that the particle tends to adopt the mode with smaller kinetic energy.

The multiple particles motions are of more interests for applications, the motion of multiple ellipsoidal particles inside tube flows will be investigated in the near future.

Acknowledgments

Huang is supported by National Natural Science Foundation of China (Grant No. 11172297), Anhui Provincial Natural Science Foundation (Grant No. 1308085MA06), Fundamental Research Funds for the Central Universities and Program for New Century Excellent Talents in University, Ministry of Education, China (NCET-12-0506).

References

[1] G. B. JEFFERY, *The motion of ellipsoidal particles immersed in a viscous fluid,* Proceedings of the Royal Society of London A: Mathematical, Physical and Engineering Sciences, The Royal Society, 102(715) (1922), pp. 161–179.

[2] C. K. AIDUN, Y. LU AND E. J. DING, *Direct analysis of particulate suspensions with inertia using the discrete Boltzmann equation,* J. Fluid Mech., 373 (1998), pp. 287–311.

[3] D. QI AND L. S. LUO, *Rotational and orientational behaviour of three-dimensional spheroidal particles in Couette flows,* J. Fluid Mech., 477 (2003), pp. 201–213.

[4] H. HUANG, X. YANG AND M. KRAFCZYK ET AL., *Rotation of spheroidal particles in Couette flows,* J. Fluid Mech., 692 (2012), pp. 369–394.
[5] Z. YU, N. PHAN-THIEN AND R. I. TANNER, *Rotation of a spheroid in a Couette flow at moderate Reynolds numbers,* Phys. Rev. E, 76(2) (2007), 026310.
[6] H. HUANG, Y. F. AND X. LU, *Shear viscosity of dilute suspensions of ellipsoidal particles with a lattice Boltzmann method,* Phys. Rev. E, 86(4) (2012), 046305.
[7] Y. CHEN, Q. KANG AND Q. CAI ET AL., *Lattice Boltzmann simulation of particle motion in binary immiscible fluids,* Commun. Comput. Phys., 18(03) (2015), pp. 757–786.
[8] G. SEGRE, *Radial particle displacements in Poiseuille flow of suspensions,* Nature, 189 (1961), pp. 209–210.
[9] A. KARNIS, H. L. GOLDSMITH AND S. G. MASON, *The flow of suspensions through tubes: V. Inertial effects,* The Canadian Journal of Chemical Engineering, 44(4) (1966), pp. 181–193.
[10] J. FENG, H. H. HU AND D. D. JOSEPH, *Direct simulation of initial value problems for the motion of solid bodies in a Newtonian fluid Part 1. Sedimentation,* J. Fluid Mech., 261 (1994), pp. 95–134.
[11] B. H. YANG, J. WANG AND D. D. JOSEPH ET AL., *Migration of a sphere in tube flow,* J. Fluid Mech., 540 (2005), pp. 109–131.
[12] M. SUGIHARA-SEKI, *The motion of an ellipsoid in tube flow at low Reynolds numbers,* J. Fluid Mech., 324 (1996), pp. 287–308.
[13] Z. YU, N. PHAN-THIEN AND R. I. TANNER, *Dynamic simulation of sphere motion in a vertical tube,* J. Fluid Mech., 518 (2004), pp. 61–93.
[14] T. W. PAN, C. C. CHANG AND R. GLOWINSKI, *On the motion of a neutrally buoyant ellipsoid in a three-dimensional Poiseuille flow,* Comput. Methods Appl. Mech. Eng., 197(25) (2008), pp. 2198–2209.
[15] P. LALLEMAND AND L. S. LUO, *Lattice Boltzmann method for moving boundaries*, J. Comput. Phys., 184(2) (2003), pp. 406–421.
[16] D. D'HUMIERES, *Multiple-relaxation-time lattice Boltzmann models in three dimensions*, Philosophical Transactions of the Royal Society of London A: Mathematical, Physical and Engineering Sciences, 360(1792) (2002), pp. 437–451.
[17] H. HUANG, X. YANG AND X. LU, *Sedimentation of an ellipsoidal particle in narrow tubes,* Phys. Fluids, 26(5) (2014), pp. 053302.
[18] Y. CHEN, Q. CAI AND Z. XIA ET AL., *Momentum-exchange method in lattice Boltzmann simulations of particle-fluid interactions,* Phys. Rev. E, 88(1) (2013), 013303.
[19] T. N. SWAMINATHAN, K. MUKUNDAKRISHNAN AND H. H. HU, *Sedimentation of an ellipsoid inside an infinitely long tube at low and intermediate Reynolds numbers,* J. Fluid Mech., 551 (2006), pp. 357–385.
[20] X. YANG, H. HUANG AND X. LU, *Sedimentation of an oblate ellipsoid in narrow tubes*, Phys. Rev. E, 92(6) (2015), 063009.
[21] D. QI, *Lattice-Boltzmann simulations of particles in non-zero-Reynolds-number flows,* J. Fluid Mech., 385 (1999), pp. 41–62.